Measurements of the $1s2s\ ^1S_0-1s2p\ ^3P_{1,0}$ transitions in heliumlike nitrogen

J. K. Thompson, D. J. H. Howie,* and E. G. Myers
Department of Physics, Florida State University, Tallahassee, Florida 32306
(Received 28 July 1997)

Using a Doppler-tuned fast ion-beam–laser technique, with co- and counterpropagating laser beams, the intercombination $1s2s\ ^1S_0-1s2p\ ^3P_{1,F}$ transitions in $^{14}N^{5+}$ and $^{15}N^{5+}$ have been measured to 0.7 ppm. This precision is equivalent to 20 ppm of the two-electron Lamb shift and is more than two orders of magnitude more precise than current relativistic and QED theoretical results at this Z. A comparison is made with theory for the hyperfine structure and isotope shift. Additionally, using a single copropagating laser beam, the differences between the $2\ ^1S_0-2\ ^3P_{1,F=1}$ and $2\ ^1S_0-2\ ^3P_0$ intervals in $^{14}N^{5+}$ and between the $2\ ^1S_0-2\ ^3P_{1,F=3/2}$ and $2\ ^1S_0-2\ ^3P_0$ intervals in $^{15}N^{5+}$ have also been measured. From the former we obtain an improved result for the $^{14}N^{5+}$ $2\ ^3P_1-2\ ^3P_0$ fine structure. [S1050-2947(98)04801-X]

PACS number(s): 32.30.Rj, 31.30.Jv, 31.30.Gs, 32.30.Bv

I. INTRODUCTION

Due to impressive advances in computational technique, the nonrelativistic two-electron atom or ion is essentially a solved problem [1]. Consequently, comparisons between theory and experiment serve to test calculations of interesting relativistic and QED effects [2–6], several of which are not present in the spectra of the one-electron system, e.g., see [7]. Because these effects in general scale as high powers of Z (as $\sim Z^4$ and $\sim Z^4 \ln Z\alpha$), laser spectroscopic measurements in heliumlike ions [8–13], though of lower precision than measurements in helium, e.g., [14–16], can provide important additional tests of theory.

As discussed in previous work on heliumlike nitrogen [8,9], the intercombination $1s2s\ ^1S_0-1s2p\ ^3P_1$ transition and the intercombination-hyperfine-induced $1s2s\ ^1S_0-1s2p\ ^3P_0$ transition are particularly sensitive to relativistic and QED effects and in some cases are amenable to precision spectroscopy with the fast beam laser technique. This is because the $1s2s\ ^1S_0-1s2p\ ^3P_1$ interval remains small, in fact in the infrared, for Z up to ~ 40. In the case of N^{5+} this interval is close to a wavelength of 10 μm and is accessible to spectroscopy with a CO_2 laser. Because of the large cancellation of the nonrelativistic energies the relativistic and QED contributions to the transition energy are as large as 19% and 3.5%, respectively. For comparison, the relativistic and QED contributions to the $2\ ^3S_1-2\ ^3P_2$ interval in helium at 1083 nm [15,16] are only 0.023% and 0.002% and in the same transition in heliumlike krypton (Kr^{34+}) at 11.1 nm [4,17] they are, respectively, 69% and 1.3%.

In the previous measurement of the total $^{14}N^{5+}$ $1s2s\ ^1S_0-1s2p\ ^3P_{1,F}$ intervals [9], the precision was mainly limited by uncertainty in the Doppler shift due to uncertainty in the beam velocity. Here, by using laser beams parallel and antiparallel to the ion beam, we have reduced the sensitivity to uncertainty in the absolute beam velocity and have obtained a tenfold improvement in precision. The measurements have also been extended to $^{15}N^{5+}$. The co- and counterpropagating laser-beam technique was not used to measure the very weak hyperfine-induced $2\ ^1S_0-2\ ^3P_0$ transitions. However, as a subsidiary measurement, the technique of Ref. [8] was used to obtain more data for the $J=0-1$ fine structure. Specifically, this was done by measuring the differences between the $2\ ^1S_0-2\ ^3P_{1,F=1}$ and $2\ ^1S_0-2\ ^3P_0$ intervals in $^{14}N^{5+}$ and between the $2\ ^1S_0-2\ ^3P_{1,F=3/2}$ and $2\ ^1S_0-2\ ^3P_0$ intervals in $^{15}N^{5+}$. By combining the present result for $^{14}N^{5+}$ with the previous measurement of the $2\ ^3P_{1,F=2}-2\ ^3P_0$ component [8], we have greatly reduced the uncertainty in the correction due to the hyperfine interaction and have obtained a small improvement in the overall result for the $2\ ^3P_1-2\ ^3P_0$ fine-structure interval.

II. EXPERIMENT

A schematic of the relevant energy levels in $^{14,15}N^{5+}$ is shown in Fig. 1 and the setup used for the present measurements is shown in Fig. 2. The basic technique is to produce

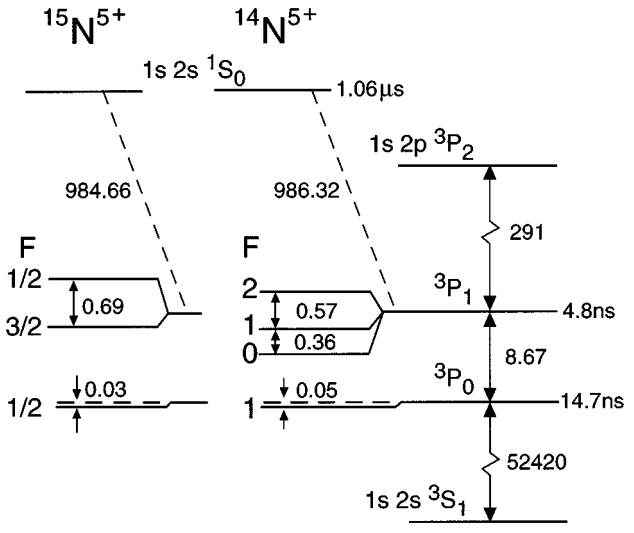

FIG. 1. Schematic of the energy levels of $^{14,15}N^{5+}$ relevant to the experiment. Approximate spacings are given in units of cm^{-1}.

*Present address: Oxford Nanotechnology Plc, Oxford Center for Innovation, Mill Street, Oxford, United Kingdom.

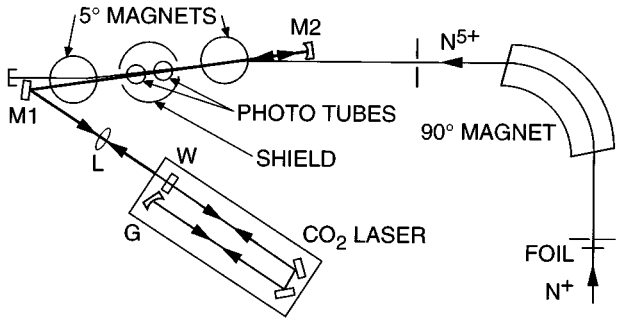

FIG. 2. Schematic of the experimental arrangement. G is the diffaction grating, W the window, L the lens, $M1$ the plane mirror, and $M2$ the concave partial reflector.

a beam of N^{5+} ions by foil stripping and magnetically analyzing a N^+ beam at energies from 5.0–6.6 MeV. Following a flight of approximately 1 μs, $\sim$0.1% of the ions are in the $2\ ^1S_0$ state, with mean lifetime 1.06 μs [19]. The ion beam is then merged collinearly with CO_2 laser radiation near 10 μm. Transitions are induced to the $2\ ^3P_{1,F}$ and $2\ ^3P_0$ levels, with mean lifetimes 4.8 ns and 14.7 ns, respectively [20,21]. The subsequent increased $2\ ^3P$–$2\ ^3S$ fluorescence at 191 nm is detected using a pair of photomultiplier tubes. Because the CO_2 laser [22] is line tunable but not continuously tunable, the resonances are scanned by varying the beam velocity, which is nearly $0.03c$, so as to vary the Doppler shift.

Previously the resonances were induced with a single laser beam counterpropagating with respect to the ion beam. Here the laser cavity has been extended to include the interaction region, enabling a particular N^{5+} resonance to be scanned sequentially using both co- and counterpropagating laser beams. In the following subsections we first discuss the reduced sensitivity to uncertainties in beam velocity obtained with this technique. We then present details of the accelerator system, the laser, the alignment procedure, the detection system and of the data, and the results obtained.

A. Doppler-tuned spectroscopy with co- and counterpropagating laser beams

Consider an ion moving with velocity $\beta_1 c$ at (a small) angle θ_1 with respect to the propagation direction of a laser beam of laboratory frequency ω_1. Treating the laser beam as a plane wave, a transition of frequency ω' will be related on resonance to ω_1 according to the relativistic Doppler formula

$$\omega' = \omega_1 \gamma_1 (1 - \beta_1 \cos\theta_1), \tag{1}$$

where $\gamma_1 = (1-\beta_1^2)^{-1/2}$. Likewise, an ion traveling at velocity $\beta_2 c$ will be resonant with a counterpropagating laser beam of frequency ω_2 if

$$\omega' = \omega_2 \gamma_2 (1 + \beta_2 \cos\theta_2), \tag{2}$$

where θ_2 is defined relative to the direction opposite to the second laser beam. If the laser is continuously tunable, then Eqs. (1) and (2) can be satisfied with $\beta_1 = \beta_2$ and $\theta_1 = \theta_2 = 0$, giving the well-known Doppler-free result [23,10,11]

$$\omega' = (\omega_1 \omega_2)^{1/2}. \tag{3}$$

If the laser frequencies ω_1, ω_2 are fixed, as in the case of the CO_2 laser, the beam velocity or interesection angle must be changed between resonances. However, if ω_1 and ω_2 can be chosen so that resonances occur at similar beam velocities with a near collinear geometry, a considerable reduction in sensitivity to the absolute beam velocity and the alignment is still obtained [23]. For $\beta_1 \simeq \beta_2 < 0.03$, $|\beta_1 - \beta_2| < 0.001$, and $|\theta_1|, |\theta_2| < 0.01$, conditions we were able to easily meet in the present experiment, the approximate result

$$\frac{\omega'^2 - \omega_1\omega_2}{\omega_1\omega_2} \simeq \Delta p + \frac{\Delta p}{2}[\Delta p - \overline{p^2} - \overline{\theta^2}] - \frac{\Delta(\theta^2)}{2}\overline{p}\left(1 + \frac{\overline{p^2}}{4}\right) + \overline{p^2}\,\overline{\theta^2}, \tag{4}$$

where $\Delta p = \gamma_2\beta_2 - \gamma_1\beta_1$, $\overline{p} = (\gamma_1\beta_1 + \gamma_2\beta_2)/2$, $\Delta(\theta^2) = \theta_2^2 - \theta_1^2$, and $\overline{\theta^2} = (\theta_1^2 + \theta_2^2)/2$, gives the transition frequency in terms of the laser frequencies to better than one part in 10^9. From Eq. (4) we see that the measurement is mainly sensitive to the change in beam rigidities between the resonances Δp and that the sensitivity to the absolute beam velocity is reduced by more than a factor of 10^4.

B. Accelerator system and ion-beam analysis

The N^+ ion beam was obtained from a radio-frequency discharge ion source [24] installed in the terminal of the Florida State University tandem Van de Graaff–Pelletron accelerator. The source gas was either natural $^{14}N_2$ or greater than 99% enriched $^{15}N_2$. The accelerated ion beam was stripped by a nominally 4-μg/cm^2 carbon foil and then analyzed by a $R = 86$ cm double focusing 90° bending magnet. For most of the data taking runs, entrance and exit slit widths of 0.5 mm were used corresponding to a nominal energy resolution of 1.8 keV full width at half maximum (FWHM) at 6 MeV. N^{5+} beam currents of 1–4 particle nA were obtained in the interaction chamber. The flight path from the foil to the interaction region was approximately 10 m.

In our previous measurements, for historical reasons, the stripper foil was located approximately 20 cm down beam of the entrance slits of the 90° bending magnet. Though the magnetic field in this region is negligible, the beam divergence introduced by the foil led to a focusing error at the 90° magnet exit slits. This limited the attainable energy resolution and also led to a significant energy variation horizontally across the ion beam in the interaction chamber. Because in those experiments the laser waist at the interaction region was narrower than the ion beam, this led to a systematic variation in the centroid energy of a laser-induced resonance, with relative horizontal alignment of the two beams, of up to 2.5 keV/mm. In the present experiment the foil has been moved up beam of the entrance slits and, depending on the slit settings, the energy spread of the ion beam can be reduced by more than a factor of 2. At the same time, the laser spot size has been increased to match that of the ion beam. As a result of these changes the apparent resonance centroid shift with relative horizontal position has been reduced to less than 0.4 keV/mm. However, because the foil is exposed to a higher beam current than previously, its useful lifetime, before significant loss of transmission through the magnet occurs, is only a few hours.

TABLE I. CO_2 laser lines and corresponding N^{5+} beam energies (to the nearest keV) used for the measurements of the $2\,^1S_0-2\,^3P_{1,F}$ transitions using co- and counterpropagating beams.

		Copropagating (9.4-μm band)		Counterpropagating (10.4-μm band)	
Isotope	F	Line	E (MeV)	Line	E (MeV)
	2	P-50	6.136	P-6	6.151
^{14}N	1	P-52	5.085	P-2	5.092
	0	P-48	6.622	P-6	6.537
^{15}N	1/2	P-52	6.437	P-8	6.531
	3/2	P-52	6.143	P-6	6.105

The current in the 90° magnet was stepped by an auxiliary current regulated power supply in parallel with the magnet's usual current regulated supply. The auxilliary supply was controlled by the data acquisition computer using a digital-to-analog converter. The magnetic field was sampled using an NMR probe and read to ± 0.01 G. Using a search routine, the computer was able to step the field in nearly evenly spaced steps of 0.1 G, equivalent to a beam energy change of about 400 eV. The magnetic field was repetitively sampled and recorded at each step.

C. Carbon dioxide laser

The laser used was a 6 m discharge length, axial flow industrial CO_2 laser that was modified by installing a 75-lines/mm, $R=20$ m, BeCu concave diffraction grating [25]. The discharge current was 20 mA and was switched at 500 Hz with a 50% duty cycle. As a convenient means of producing counterpropagating beams and obtaining useful laser power on relatively low gain laser lines, the laser cavity was extended to include the laser-ion interaction region. This was achieved by replacing the laser output coupler with a ZnSe window, by using a 0.87-m focal-length GaAs lens as the window where the laser beam enters the interaction chamber, and by completing the cavity with a 0.70-m radius-of-curvature Ge mirror. This mirror had a nominal transmission of 1% and enabled the intracavity power and mode to be monitored. GaAs was chosen for the lens, despite its higher absorption compared to ZnSe, because of the need to block visible light from the CO_2 discharge from reaching the photomultiplier tubes in the interaction chamber. The total length of the extended laser cavity was 10.5 m. The CO_2 laser lines used for the various $^{14,15}N^{5+}$ $1s2s\,^1S_0-1s2p\,^3P_{1,F}$ intervals and the approximate beam energies at which the resonances occur are shown in Table I. The laser lines and beam energies used for the fine-structure measurements are shown in Table II.

TABLE II. CO_2 laser lines and corresponding N^{5+} beam energies (to the nearest keV) used for the fine-structure measurements. Laser lines are from the 9.4-μm band and the laser is copropagating in all cases.

		$2\,^1S_0-2\,^3P_{1,F}$		$2\,^1S_0-2\,^3P_0$	
Isotope	F	Line	E (MeV)	Line	E (MeV)
^{14}N	1	P-52	5.085	P-44	5.075
^{15}N	3/2	P-54	5.266	P-46	5.282

The cavity extension was designed so as to keep the nominal TEM_{00} laser mode within the discharge region unchanged, while producing an intracavity beam waist of approximate diameter 1 mm located a few centimeters up beam of the center of the interaction chamber. However, in practice, with this geometry a pure TEM_{00} mode was not obtained, and by using a lens and a series of apertures following the partial reflector, the spot size at the waist was determined to be between a factor of 1.5 and 2 larger than the simple Gaussian beam prediction. The higher gain lines used from the 10.4-μm band gave a larger spot size than the lower gain lines from the 9.4-μm band. In addition, the intracavity powers (averaged over the 1 ms of the laser pulse) were between 100 and 300 W. Hence, at least for the higher gain lines, there was no improvement in the power at the interaction region compared to the use of the laser with an output coupler as in the previous work. This behavior is presumably due to the fact that, in such a long, high gain laser, waveguide effects are important and with the cavity modification, higher-order and unstable modes are able to lase and compete for the available gain. Nevertheless, the powers and mode quality were adequate for the present measurements.

The longitudinal mode spacing of the extended cavity was approximately 14 MHz and so at any instant the laser frequency was within 7 MHz of the center of the gain profile. In fact, because the laser cavity was unstabilized the position of the lasing mode or modes would drift with the result that the time average was much closer to the centroid of the gain profile. Since the pressure shifts of the laser transitions in the 20-torr 9%:13.5%:77.5% CO_2:N_2:He gas mixture used are less than 2 MHz [26], we conservatively estimate that the average laser output frequency, over the duration of a particular sequence of scans, was within 3 MHz of the respective standard CO_2 transition frequencies as given in Ref. [27].

D. Alignment procedure

Our procedure for obtaining collinear alignment of the laser and ion beams made use of two copper aperture plates, mounted on vacuum feedthroughs, spaced 18 cm apart, symmetrically up beam and down beam of the center of the interaction chamber. Each aperture plate was drilled with holes 1.25 mm and 2.5 mm diameter, spaced 6 mm apart along the direction of feedthrough insertion. After a certain laser line had been selected and optimized by adjustment of the laser optics, each feedthrough in turn would be inserted and adjusted until the 2.5-mm aperture was centered on the laser

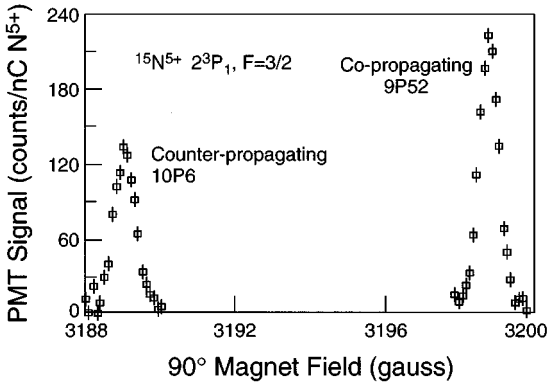

FIG. 3. Single energy scan of the $1s2s\ ^1S_0-1s2p\ ^3P_{1,F=3/2}$ transition in $^{15}N^{5+}$ excited with co- and counterpropagating laser beams.

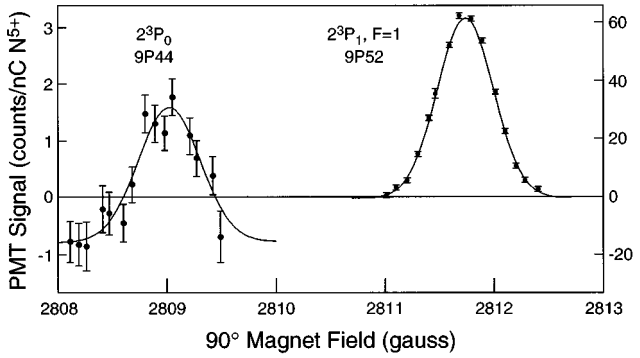

FIG. 4. Composite of three scans of the $1s2s\ 1S_0-1s2p\ ^3P_{1,F=1}$ transition and the hyperfine-induced $1s2s\ ^1S_0-1s2p\ ^3P_0$ transition in $^{14}N^{5+}$ excited with copropagating laser beams.

beam, as indicated by minimum reduction in laser power. By changing the feedthrough insertion with precision shims, the 1.25-mm-diam apertures were then located on the same center to better than ± 0.05 mm. The ion beam was then aligned and focused through both 1.25-mm apertures using two pairs of magnetic deflectors and a magnetic quadrupole doublet focusing lens. Typically 50% of the ion beam could be transmitted through the pair of small apertures, depending on the foil condition. The apertures were fully withdrawn from the beam path during data taking.

Auxilliary measurements of the stability of the ion- and laser-beam alignment were made as follows. Using an ion-beam position monitor consisting of a pair of slits on a precision travel, the horizontal translation of the ion beam at the interaction region with increasing energy was measured to be less than 0.01 mm/keV. The position of the laser-beam mode inside the chamber was also monitored. This was done by locating the position of the waist formed outside the interaction chamber by a lens placed after the partial reflector. By tracking the position of this ''image'' waist we determined that the horizontal motion of the waist at the interaction region, as laser lines were changed, was less than 0.1 mm.

E. Detection system

The detection system consisted of two, 25-mm-diam photomultiplier tubes with CsTe photocathodes and silica windows, with a nominal quantum efficiency of 15% at 190 nm. The tubes were positioned 17 mm above the ion beam and 75 mm apart. The detection efficiency was more than doubled by placing MgF_2 overcoated aluminized mirrors under the ion beam to focus light emitted downward back towards the phototubes. To reduce perturbing electric fields at the ion beam, the phototubes viewed the ion beam through grounded metal grids. The detectors and the beam path between the magnets were surrounded by magnetic shielding, providing a 15-cm path up beam of the observation region where the magnetic field was less than 2 G. The interaction region was pumped by a 350-L/s turbomolecular pump and the nominal chamber vacuum was 3×10^{-7} mbar, dominated by water vapor. The shield and detectors were cooled to around $-10\,^{\circ}$C, reducing the phototube dark count rates to around 10 Hz.

Laser-induced fluorescence signals ranged from ~ 1 kHz/particle nA for the strongest resonances down to a few Hz/particle nA for the hyperfine-induced resonances. Combined with estimates of the transition probability and detection efficiency, these rates are consistent with $\sim 0.3\%$ of the N^{5+} ions being formed at the foil in the $2\ ^1S_0$ state. These signals were seen on top of various backgrounds. First, there was an ion-beam induced rate of about 100 Hz/particle nA. Since cooling the shield to liquid-nitrogen temperature did not significantly reduce this, it is likely that this background is not due to collisions with the residual gas but is due to some sensitivity of our detection system to soft-x-ray fluorescence from $2\ ^1S_0$ and $2\ ^3S_1$ metastable states in the ion beam. Second, and more troublesome, there was a variable laser-induced background, $\sim 10-1000$ Hz, due to light emitted from ''hot spots'' on the laser optics. In order to subtract this laser-induced background, the ion beam was switched at 1 Hz with an electrostatic deflector and the signal S was obtained from the double difference

$$S=(N_{on}-N_{off})_{ions\ on}-(N_{on}-N_{off})_{ions\ off}, \qquad (5)$$

where N_{on}, N_{off} are the counts recorded in the laser on and laser off intervals, respectively. Third, at the level of a few Hz/particle nA, this double difference signal also suffered from a small offset that was significant when searching for the weak hyperfine-induced resonances. The offset was usually negative, implying a reduction in count rate due to the laser. We verified that this background was due to a genuine laser–ion-beam interaction by observing its falloff as the laser and ion beams were deliberately misaligned. However, the small size of the effect made it difficult to study and it is not presently understood. We note that nonresonant laser-induced backgrounds were also observed in the CO_2 laser resonance measurements of the fine structure of F^{7+} [13]. There it was suggested that they originated from the interaction of the laser radiation with long-lived Rydberg states [28].

F. Data

The resonance pairs indicated in Tables I and II were scanned by stepping the 90° magnet field in a series of looping up and down scans. For the $2\ ^3P_1$ resonances typical integration times were 10 s a point, while for the $2\ ^3P_0$ resonances this was increased to 50 or 100 s a point. An example

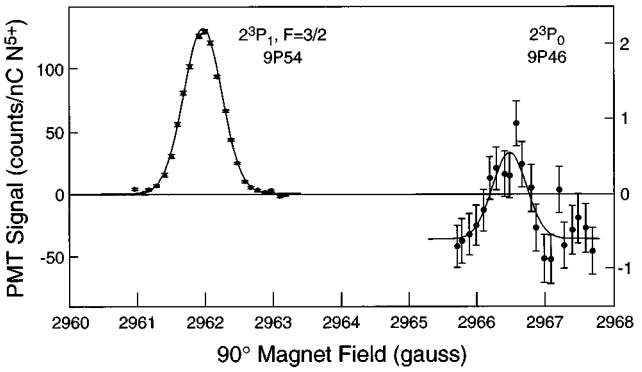

FIG. 5. Composite of four scans of the $1s2s\ ^1S_0-1s2p\ ^3P_{1,F=3/2}$ transition and the hyperfine-induced $1s2s\ ^1S_0-1s2p\ ^3P_0$ transition in $^{15}N^{5+}$ excited with copropagating laser beams.

of a single scan from the co- and counterpropagating laser beam data is shown in Fig. 3. The averages of all the scans used for the fine-structure measurements are shown in Figs. 4 and 5. Because of the lower laser intensity and beam current and higher backgrounds, the present setup was not optimal for observing the weak hyperfine-induced resonances and the signal-to-noise ratio obtained was poorer than obtained previously [8]. Nevertheless, for both resonances the statistics we were able to obtain in the available beam time were adequate for useful information to be extracted. For most of the resonance data used in the measurements the observed widths were between 2.0 and 2.8 keV (FWHM), depending on the details of slit settings, beam tuning, and foil condition. The narrowest resonance (see Fig. 6) was obtained with magnet slit widths of 0.2 mm and had a FWHM of 1.2 keV. This corresponds to 0.003 cm^{-1}, which can be compared with the natural transition width of 0.0011 cm^{-1}. In order to obtain centroids the resonances were fitted with Gaussians on flat backgrounds. Although in some cases the statistics were sufficient that the Lorentzian component to the line shape was evident, the use of a more complex fitting function had a negligible effect on the location of the centroids. Asymmetry in the line shapes, stemming from the velocity distribution of the ions and the details of the laser

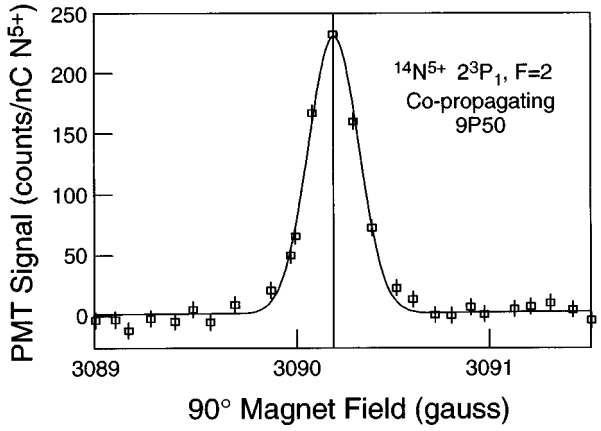

FIG. 6. Single energy scan of the $1s2s\ ^1S_0-1s2p\ ^3P_{1,F=2}$ transition in $^{14}N^{5+}$ obtained with 0.2-mm-wide analyzing magnet slits.

TABLE III. Results for the $^{14,15}N^{5+}$ $2\ ^1S_0-2\ ^3P_{1,F}$ transition wave numbers.

$^{14}N^{5+}$		$^{15}N^{5+}$	
F	E (cm^{-1})	F	E (cm^{-1})
2	986.0062(7)	1/2	984.1830(7)
1	986.5799(7)	3/2	984.8754(7)
0	986.9440(7)		

interaction, was found to be small. Since to first order any asymmetry is common to both resonances in a pair, its effect was negligible in the centroid differences compared to other systematic errors.

In addition to the co- and counterpropagating beam measurements, the individual $2\ ^1S_0-2\ ^3P_{1,F}$ resonances in $^{14,15}N^{5+}$ were scanned in a continuous energy scan, using a single laser line (10.4-μm P-6). This procedure, which was used previously [8], gives results for the hyperfine intervals that can be compared with those obtained by differencing the results of the co- and counterpropagating beam measurements.

G. Results

The wave numbers obtained for the five $^{14,15}N^{5+}$ $2\ ^1S_0-2\ ^3P_{1,F}$ transitions are shown in Table III. The contributions to the assigned errors are shown in Table IV. The procedure for obtaining these results was as follows. First, we converted the averages of the resonance centroids in gauss into beam rigidities p using a pre-existing magnet calibration based on a well-known proton-induced resonance [29]. Then using Eq. (4) and the data obtained with co- and counterpropagating beams, we obtained preliminary results for the five transition wave numbers. The statistical error shown in Table IV was obtained from the distribution of the results for different scans. To obtain an improved value for the differential magnet calibration in the region of our measurements, we compared the differences between the hyperfine intervals obtained by differencing these results with the hyperfine intervals obtained from those measurements where a single, counterpropagating laser line was used. Because these latter measurements involved scanning much larger energy intervals (386 and 287 keV for ^{14}N and ^{15}N, respectively), they are far more sensitive to the magnet calibration and can be used to obtain it if the hyperfine splittings are known. We therefore did a least-squares fit to the hyperfine interval measurements obtained by both methods, allowing the differential magnet calibration constant to be a free parameter. The

TABLE IV. Error estimates for the results in Table III. Units are 10^{-5} cm^{-1}.

statistical	$\leqslant 10$
magnet calibration	$\leqslant 22$
dE/dx	17
misalignment	20
divergence	62
total	$\leqslant 72$

TABLE V. Results for the $^{14,15}N^{5+}$, $2\ ^3P_{1,F-F'}$ hyperfine intervals. Units are cm^{-1}.

Isotope	F-F'	ΔE
$^{14}N^{5+}$	2-1	0.5737(7)
$^{14}N^{5+}$	1-0	0.3642(7)
$^{14}N^{5+}$	2-0	0.9378(7)
$^{15}N^{5+}$	1/2-3/2	0.6925(7)

result was an increase in dp/dB of $2.0(4)\times10^{-3}$ and that all the hyperfine results were brought into agreement with a maximum discrepancy of 4×10^{-4} cm^{-1}. Because the energy intervals involved in the co- and counterpropagating measurements were small, the resulting systematic corrections to the total wave numbers were at most 2.2×10^{-4} cm^{-1}. Since there is some uncertainty in the reproducibility of this calibration correction, we include an uncertainty equal to this correction in each case, as indicated in the second row of Table IV.

The other contributions to the errors are as follows: The ''dE/dx'' contribution takes account of possible variation in energy across the ion beam coupled with possible systematic shifts, between a resonance pair, of the location of the ion beam ($\leqslant$0.2 mm) and the laser beams ($\leqslant$0.1 mm) at the interaction region. The misalignment uncertainty contribution is based on a maximum change in the angular offset between the laser- and ion-beam axes of 5 mrad. The divergence contribution takes account of wave front curvature effects associated with the multitransverse mode laser beam and the fact that the mode quality was significantly worse for the longer wavelength lines of the 10.6-μm band, which was used for the counterpropagating beam. We estimated this contribution by assuming that the divergence of the counterpropagating beam is limited only by the aperture at the intracavity lens and has a root-mean-square divergence of 9 mrad. Indirect evidence that these effects have not been underestimated comes from the lack of systematic offsets, at the level of 2×10^{-4} cm^{-1}, between the resonance centroids obtained from the different detectors. No attempt was made to analyze the output frequency of our unstabilized CO_2 laser, but we do not expect any *systematic* shifts between its average output frequency on a given line and the reference data of [27] at the 10^{-4}-cm^{-1} level.

TABLE VI. Results for the two measured $^{14,15}N^{5+}$ $2\ ^3P_{1,F}-2\ ^3P_0$ fine-structure intervals. Units are cm^{-1}.

$^{14}N^{5+}$ $^3P_{1,F=1}$-$^3P_0$	$^{15}N^{5+}$ $^3P_{1,F=3/2}$-$^3P_0$
8.4596(8)	8.4863(9)

The hyperfine intervals obtained by taking the differences of the results in Table III are shown in Table V. Our error estimates take account of the statistical errors and correlations between the magnet calibration corrections shown in Table IV. To simply combine the systematic errors shown in the last three rows of Table IV would overestimate these contributions since a considerable fraction is expected to be common to all the measured hyperfine components. This degree of commonality is difficult to estimate, but we believe it is reasonable to take it to be 50%.

The results for the two measured fine-structure intervals are given in Table VI. The assigned errors are based on statistical fitting errors of 3×10^{-4} and 4×10^{-4} cm^{-1} for the two hyperfine-induced resonances and allowances for the effects of possible energy variation across the ion beam ($\sim3\times10^{-4}$ cm^{-1}), angular offsets ($\sim2\times10^{-4}$ cm^{-1}), and for wave-front curvature ($\sim7\times10^{-4}$ cm^{-1}). Because of the smallness of the energy intervals between the resonances, the contributions from uncertainty in the magnet calibration were less than 10^{-4} cm^{-1}.

III. DISCUSSION

A. Hyperfine structure

In Table VII we compare our present measurements of the $^{14,15}N^{5+}$ $2\ ^3P_1$ hyperfine intervals with our previous measurements in $^{14}N^{5+}$ [8], with the recent relativistic configuration interaction calculations of Johnson *et al.* [18], and with the nonrelativistic calculations of Ohtsuki and Hijikata [30]. In the first row we present the results of Johnson *et al.* We note that these calculations, though allowing for relativistic effects, do not make allowance for QED corrections and also use a calculated value for the fine structure of 8.735 cm^{-1} versus the experimental value of 8.671 cm^{-1} [8] (and see below). In the second row we make an approximate allowance for QED by scaling the effective hyperfine coupling constant by $(g_s-2)/2\simeq\alpha/2\pi$ and for the use of the experi-

TABLE VII. Comparison of theory and experiment for the the $^{14,15}N^{5+}$ $2\ ^3P_{1,F-F'}$ hyperfine intervals. Units are cm^{-1}.

Source \ F-F'	$^{14}N^{5+}$ 2-1	$^{14}N^{5+}$ 1-0	$^{14}N^{5+}$ 2-0	$^{15}N^{5+}$ 1/2-3/2
Johnson *et al.* [18]	0.574 43	0.362 81	0.937 24	0.692 95
QED, ΔE_{01}	0.000 24	0.000 85	0.001 09	0.001 10
Quadrupole	−0.000 51	0.001 28	0.000 77	
Nuclear size	−0.000 46	−0.000 36	−0.000 82	−0.000 65
Johnson *et al.* plus corrections	0.573 7	0.364 6	0.938 3	0.693 4
Ohtsuki and Hijikata [30] plus corrections	0.573 8	0.364 7	0.938 6	0.693 6
Myers *et al.* [8]	0.572 6(7)	0.364 4(7)		
This work	0.573 7(7)	0.364 2(7)	0.937 8(7)	0.692 5(7)

TABLE VIII. Results for the two $^{14,15}N^{5+}$ $2\,^1S_0-2\,^3P_1$ intervals corrected for hyperfine structure. Units are cm^{-1}.

$^{14}N^{5+}$	$^{15}N^{5+}$
986.3180(7)	984.6557(7)

mental value of the fine structure, which shifts the ^{14}N $F=1$ level upward by 3.7×10^{-4} cm^{-1}. In the third row we give estimates for the shifts due to the quadrupole interaction in ^{14}N using the expression given in [10] and the hyperfine matrix elements of Ohtsuki and Hijikata [30] with $Q(^{14}N)=0.020\,44\times10^{-28}$ cm^2 [31]. In the fourth row we give estimates for the nuclear size (Zemach) correction, again using the expression in Ref. [10] and values for the rms nuclear charge radii from Refs. [32,33]. The total hyperfine intervals based on Johnson *et al.* are shown in the fifth row. In the sixth row we present corresponding estimates based on the results of Ohtsuki and Hijikata [30], with relativistic corrections according to the expression presented in Riis *et al.* [10,34]. The last two rows give the experimental results of Ref. [8] and for convenience the results of this work from Table V.

As can be seen from Table VII, the two theoretical results agree at the level of 3×10^{-4} cm^{-1} and can be brought into closer agreement by reducing the size of the relativistic corrections applied to the results of Ohtsuki and Hijikata by ~300 ppm. The agreement of the experimental results with the theory is also reasonable, bearing in mind the approximate nature of the QED and Zemach corrections. The apparent hyperfine anomaly of ^{15}N with respect to ^{14}N is probably not statistically significant, although it has the same sign and equivalent magnitude as that between ^7Li and ^6Li as noted in Ref. [10].

B. $^{14,15}N^{5+}$ $2\,^1S_0-2\,^3P_1$ wave numbers and isotope shift

Using the corrected hyperfine results of Johnson *et al.* we obtained results for the $2\,^1S_0-2\,^3P_1$ intervals in the absence of hyperfine interaction, which are presented in Table VIII. The procedure involved taking the $2F+1$ weighted average of the individual components and the overall hyperfine corrections cancel to first order. The result for ^{14}N is in agreement, but a factor of 10 more precise than our earlier result of 986.321(7) cm^{-1} [9]. Except to note that the closest theoretical result to our knowledge, 986.579 cm^{-1} [3], differs by 370 experimental standard deviations, the comparison with theory presented in Ref. [9] will not be repeated.

TABLE IX. Comparison of theory and experiment for the $^{14,15}N^{5+}$ $2\,^1S_0-2\,^3P_1$ isotope shift. The notation is from Ref. [1].

Contribution	ΔE (cm^{-1})
Nonrelativistic reduced mass δE_{NR}	0.0029
Relativistic reduced mass δE_{rel}	−0.0005
Mass polarization $\delta E_M{}^{(1)}$	−1.6697
Nuclear volume δE_{nuc}	0.0033(9)
Theory total	−1.6640(9)
Experiment	−1.6623(10)

TABLE X. Our results for the $^{14}N^{5+}$ $2\,^3P_0-2\,^3P_1$ fine-structure interval compared with recent theory.

Source	ΔE_{01} (cm^{-1})
This work	8.6707(7)
Yan and Drake [37]	8.68213(2)
Zhang, Yan, and Drake [38]	8.686(20)

In Table IX we compare our experimental result for the $^{14,15}N^{5+}$ $2\,^1S_0-2\,^3P_1$ isotope shift with a theoretical estimate based on the ''unified theory'' calculations of Drake [1,3]. The first and second entries in the table give, respectively, the nonrelativistic and relativistic reduced mass contributions, while the third gives the unusually large specific mass shift or ''mass polarization'' contribution to first order. These are all obtained by appropriate scaling from the results for ^{14}N given by Drake, using the masses of $^{14,15}N$ [35]. Similarly, we obtained the nuclear volume shift by scaling from the volume shift given there, using rms nuclear charge radii for ^{14}N of 2.560(11) fm [32] and for ^{15}N of 2.612(9) fm [33]. The error given for our theoretical estimate is that corresponding to the errors in these charge radii. The small discrepancy between experiment and theory is presumably due to the omission of second-order mass polarization contributions, of the two ''relativistic recoil'' contributions, and of the mass dependence of the QED contribution. We also note that the present experimental result for the isotope shift is in excellent agreement with a previous measurement of $-1.663(3)$ cm^{-1} [36]. This was obtained by measuring energy intervals between resonances in beams of ^{14}N and ^{15}N obtained sequentially from the accelerator with a mixture of isotopes in the ion source gas.

C. Fine structure

Using the corrected hyperfine structure results of Johnson *et al.* as used in the fifth row of Table VII we obtain a hyperfine contribution of 0.210 86 cm^{-1} to the $^{14}N^{5+}$ $2\,^3P_{1,F=1}-2\,^3P_0$ transition. Combining this with the experimental result in Table VI implies a hyperfine-corrected result for the $2\,^3P_1-2\,^3P_0$ fine structure ΔE_{01} of 8.6704(8) (hyperfine-structure correction) cm^{-1}, where we estimate the error from the uncertainty in the hyperfine-structure (hfs) correction to be $\sim2\times10^{-4}$ cm^{-1}. Using the previously measured value of the $^{14}N^{5+}$ $2\,^3P_{1,F=2}-2\,^3P_0$ interval [8], viz., 9.0339(7) cm^{-1}, and the corresponding correction of $-0.362\,84$ cm^{-1}, we obtain $\Delta E_{01}=8.6711(7)$ (hfs) cm^{-1}, which is in agreement. The uncertainty in the hyperfine correction to the simple average of the fine-structure results should cancel to less than 10^{-4} cm^{-1} and so we give $^{14}N^{5+}$ $\Delta E_{01}=8.6707(7)$ cm^{-1} as our final result. The good agreement between the result derived from this work and that of Ref. [8], bearing in mind the different propagation directions, laser arrangements, and beam energies, adds confidence that important systematic errors have not been underestimated. For the $^{15}N^{5+}$ $2\,^3P_{1,F=3/2}-2\,^3P_0$ interval the hfs correction is $-0.185\,45$ cm^{-1}, leading to $^{15}N^{5+}$ $\Delta E_{01}=8.6717(10)$ cm^{-1}.

In Table X we compare our combined result for $^{14}N^{5+}$ ΔE_{01} with the high-precision theoretical results of Drake and collaborators [37,38]. The first theoretical entry includes

relativistic and QED terms to $O(\alpha^4)$ a.u., while the second includes additional terms of $O(\alpha^5\ln\alpha)$ with an error estimate corresponding to the remaining uncalculated terms of $O(\alpha^5)$. We see that the experimental result presented here is sensitive to these remaining terms at the 5% level.

IV. CONCLUSION

This work demonstrates that laser spectroscopy of few electron ions produced by *foil stripping* accelerated ion beams is capable of precision at the sub-ppm level. By using co- and counterpropagating laser beams and measuring small energy differences, uncertainties caused by the Doppler effect are greatly reduced. In this experiment the major limitation in precision stemmed from poor control of the laser mode and we note that this can be addressed by techniques involving spatial filtering or resonant ''buildup'' cavities [39].

Our experimental results are in good agreement with the recent relativistic hyperfine-structure calculations of Johnson *et al.* and the experimental precision is at a level where QED, nuclear size, and nuclear quadrupole effects are significant. In N^{5+} the QED contribution to the $2\,^1S_0-2\,^3P_1$ interval is approximately 3.5% and the experimental precision is capable of testing this to 20 ppm. However, before the comparison can be made at this level, major developments in the calculation of J-independent QED and relativistic corrections are required. For the isotope shift there is significant cancellation of these theoretical uncertainties and reasonable agreement is found with an estimate deduced from the results of Ref. [3]. With an improved calculation our measurement can yield another value for the change in nuclear mean-square charge radius between ^{14}N and ^{15}N. For the $J=1-0$ fine structure, the present experimental result confirms that presented in Ref. [8] and a combined result, with a negligible uncertainty contribution from hyperfine structure, was obtained. This result should be significant for verifying the $O(\alpha^5)$ a.u. contributions to the theory, which will be required to enable a value for the fine-structure constant to be extracted from the fine structure of helium [37,40].

ACKNOWLEDGMENTS

The authors wish to thank Professor J. D. Silver for many interesting discussions, for contributions to earlier stages of the work, and for his great generosity in supplying the CO_2 laser that made this experiment possible. We also thank Professor W. R. Johnson for discussions concerning hyperfine structure and for supplying results for heliumlike nitrogen. Contributions from the staff and students of the Florida State University Superconducting Linear Accelerator Laboratory are also acknowledged. This work was partly supported by the U.S. National Science Foundation, the State of Florida, the NATO Collaborative Research Program, and the United Kingdom Science Research Council.

[1] G. W. F. Drake, in *Long Range Casimir Forces: Theory and Recent Experiments in Atomic Systems*, edited by F. S. Levine and D. Micha (Plenum, New York, 1993).
[2] G. W. F. Drake, I. B. Khriplovich, A. I. Milstein, and A. S. Yelkhovsky, Phys. Rev. A **48**, R15 (1993).
[3] G. W. F. Drake, Can. J. Phys. **66**, 586 (1988).
[4] D. R. Plante, W. R. Johnson, and J. Sapirstein, Phys. Rev. A **49**, 3519 (1994).
[5] M. H. Chen, K. T. Cheng, and W. R. Johnson, Phys. Rev. A **47**, 3692 (1993).
[6] K. T. Cheng, M. H. Chen, W. R. Johnson, and J. Sapirstein, Phys. Rev. A **50**, 247 (1994).
[7] T. Zhang and G. W. F. Drake, Phys. Rev. A **54**, 4882 (1996).
[8] E. G. Myers, D. J. H. Howie, J. K. Thompson, and J. D. Silver, Phys. Rev. Lett. **76**, 4899 (1996).
[9] E. G. Myers, J. K. Thompson, E. P. Gavathas, N. R. Claussen, J. D. Silver, and D. J. H. Howie, Phys. Rev. Lett. **75**, 3637 (1995).
[10] E. Riis, A. G. Sinclair, O. Poulsen, G. W. F. Drake, W. R. C. Rowley, and A. P. Levick, Phys. Rev. A **49**, 207 (1994).
[11] T. J. Scholl, R. Cameron, S. D. Rosner, L. Zhang, R. A. Holt, C. J. Sansonetti, and J. D. Gillaspy, Phys. Rev. Lett. **71**, 2188 (1993).
[12] T. P. Dinneen, N. Berrah-Mansour, H. G. Berry, L. Young, and R. C. Pardo, Phys. Rev. Lett. **66**, 2859 (1991).
[13] E. G. Myers, P. Kuske, H. J. Andrae, I. A. Armour, N. A. Jelley, H. A. Klein, J. D. Silver, and E. Traebert, Phys. Rev. Lett. **47**, 87 (1981); E. G. Myers, Nucl. Instrum. Methods Phys. Res. B **9**, 662 (1985).
[14] K. S. E. Eikema, W. Ubachs, W. Vassen, and W. Hogervorst, Phys. Rev. A **55**, 1866 (1997).
[15] D. Shiner, R. Dixson, and P. Zhao, Phys. Rev. Lett. **72**, 1802 (1994); R. Dixson and D. Shiner, Bull. Am. Phys. Soc. **39**, 1059 (1994).
[16] F. S. Pavone, F. Marin, P. De Natale, M. Ignuscio, and F. Biraben, Phys. Rev. Lett. **73**, 42 (1994).
[17] S. Martin, A. Denis, M. C. Buchet-Poulizac, J. P. Buchet, and J. Desesquelles, Phys. Rev. A **42**, 6570 (1990).
[18] W. R. Johnson, K. T. Cheng, and D. R. Plante, Phys. Rev. A **55**, 2728 (1997); W. R. Johnson (private communication).
[19] G. W. F. Drake, G. A. Victor, and A. Dalgarno, Phys. Rev. **180**, 25 (1969).
[20] C. D. Lin, W. R. Johnson, and A. Dalgarno, Phys. Rev. A **15**, 154 (1977).
[21] B. Schiff, C. L. Pekeris, and Y. Accad, Phys. Rev. A **4**, 516 (1971).
[22] W. J. Witteman, *The CO_2 Laser* (Springer-Verlag, Berlin, 1987).
[23] R. A. Holt, S. D. Rosner, T. D. Gaily, and A. G. Adam, Phys. Rev. A **22**, 1563 (1980).
[24] E. G. Myers, J. K. Thompson, P. A. Allen, P. E. Barber, G. A. Brown, V. S. Griffin, B. G. Schmidt, and S. Trimble, Nucl. Instrum. Methods Phys. Res. A **372**, 280 (1996).
[25] E. Bernal and R. McClellan, Appl. Opt. **15**, 2956 (1976).
[26] K. L. Soohoo, C. Freed, J. E. Thomas, and H. A. Haus, IEEE J. Quantum Electron. **QE-21**, 1159 (1985).
[27] L. C. Bradley, K. L. Soohoo, and C. Freed, IEEE J. Quantum Electron. **QE-22**, 234 (1986).

[28] P. Kuske, Doctoral dissertation, Freie Universitaet, Berlin, 1982 (unpublished).
[29] E. Huenges, H. Vonach, and J. Labetzki, Nucl. Instrum. Methods **121**, 307 (1974).
[30] K. Ohtsuki and K. Hijikata, J. Phys. Soc. Jpn. **57**, 4150 (1988).
[31] M. Tokman, D. Sundholm, P. Pyykkö, and J. Olsen, Chem. Phys. Lett. **265**, 60 (1997).
[32] L. A. Schaller, L. Schellenberg, A. Ruetschi, and H. Schneuwly, Nucl. Phys. A **343**, 333 (1980).
[33] J. W. de Vries, D. Doornhof, C. W. de Jager, R. P. Singhal, S. Salem, G. A. Peterson, and R. S. Hicks, Phys. Lett. B **205**, 22 (1988).
[34] The corrected hyperfine intervals based on Ohtsuki and Hijikata's theory differ slightly from those presented in Ref. [8] because of the use of more recent values for the magnetic dipole and quadrupole moments of ^{14}N in the present work.
[35] *Table of Isotopes*, edited by R. B. Firestone and V. S. Shirley (Wiley, New York, 1996).
[36] N. R. Claussen, J. K. Thompson, D. J. H. Howie, and E. G. Myers (unpublished).
[37] Z.-C. Yan and G. W. F. Drake, Phys. Rev. Lett. **74**, 4791 (1995); G. W. F. Drake (private communication).
[38] T. Zhang, Z.-C. Yan, and G. W. F. Drake, Phys. Rev. Lett. **77**, 1715 (1996).
[39] M. S. Fee, S. Chu, A. P. Mills,Jr., R. J. Chichester, D. M. Zuckerman, E. D. Shaw, and K. Danzmann, Phys. Rev. A **48**, 192 (1993).
[40] T. Kinoshita, Rep. Prog. Phys. **59**, 1459 (1996).